Mine Water and the Environment (2021) 40:606–621
https://doi.org/10.1007/s10230-021-00761-7

TECHNICAL ARTICLE

Monitoring Acid Mine Drainage's Effects on Surface Water in the Kizel Coal Basin with Sentinel-2 Satellite Images

Sergey V. Pyankov[1] · Nikolay G. Maximovich[1] · Elena A. Khayrulina[1] · Olga A. Berezina[1] · Andrey N. Shikhov[1] · Rinat K. Abdullin[1]

Received: 24 April 2020 / Accepted: 4 February 2021 / Published online: 18 February 2021

Abstract
Mining in the Kizel coal basin (Perm Region, Russia) ceased 20 years ago; however, AMD with high levels of total iron (Fe_{total}) and trace elements still affects the rivers. In this study, we attempted to estimate inter-annual and seasonal variability of AMD-related surface water contamination using Sentinel-2 images from 2016 to 2019. The acid mine water index (AMWI), which is a normalized difference of spectral reflectance in the red and blue bands, was calculated from Sentinel-2 images. We compared the AMWI values with measured Fe_{total} concentrations in the surface water. A statistically significant (at a 0.05 significance level) Spearman's rank correlation between AMWI and Fe_{total} concentration was found for 5 out of 7 surface water sampling points. We found that surface water contamination reaches a seasonal maximum in July, 1–1.5 months after the end of the snowmelt high water period. Excessive summer rainfalls also contributes to increased contamination, causing contamination to possibly spread more than 200 km from the AMD sources. In contrast, arid summer conditions were associated with a substantially decreased AMD discharge and Fe_{total} concentrations in the surface water. The main uncertainties in our results are associated with the effect of contaminated bottom and bank sediments and suspended sediments on the spectral characteristics of the water surface, and the relatively coarse (10 m) spatial resolution of Sentinel-2 images. However, despite the data and method limitations, our results show that Sentinel-2 images have substantial potential for monitoring AMD-related contamination of surface water.

Keywords Coal mining areas · Acid mine water · Surface water contamination · Inter-annual and seasonal variability · Remote sensing data · Spectral indices

Introduction

Surface water contamination caused by acid mine drainage (AMD) is one of the biggest environmental problems caused by the mining of coal and other sulphide-rich mineral deposits (Sarmiento et al. 2009). When AMD flows into natural water, precipitates (mostly ferric hydroxide and hydrosulfate and aluminium hydroxide) (Valente et al. 2009; Menshikova et al. 2020; Wolkersdorfer et al. 2020). The sediments are considered to be a secondary pollution source and can spread downstream for long distances (Powell et al. 1988; Siddharth et al. 2002, Tao et al. 2012). Besides AMD, the leaching of waste rock dumps also contributes to the pollution of surface water. This process is intensified by increased surface runoff during snowmelt and heavy rainfalls (Maximovich and Pyankov 2018).

AMD and runoff from rock dumps are typical for coal mining areas worldwide (Burrell et al. 2000; Donovan et al. 2003; Okamoto et al. 2006). Abandoned mines can also be pollution sources, since they are often flooded with groundwater. AMD from underground coal mines can persist for more than 100 years, with little change in chemical composition (Demchak et al. 2004; Johnson and Hallberg 2005).

Earth remote sensing (ERS) data can substantially improve environmental monitoring in coal mining areas. Imaging spectroscopy can be considered as a substantial addition or alternative to conventional methods (based on chemical analyses) and as an efficient way to estimate AMD-related contamination (Kopačková 2019). Many researchers have successfully used ERS data to detect AMD, to assess the spectral characteristics of secondary minerals formed

✉ Andrey N. Shikhov
and3131@inbox.ru

[1] Perm State University, 15 Bukireva Str, 614990 Perm, Russia

during acidification and to estimate the degree of surface water pollution (Anderson and Robbins 1998; Raval 2011; Seifi et al. 2019).

Landsat (MSS) satellite images have been used to assess the environmental settings in mining areas and to detect large sources of AMD since the 1970s (Alexander et al. 1973; Wobber et al. 1975). It was found that AMD as well as technogenic sediment formed during acidification had higher spectral reflectance in the wavelength range 650–750 nm, compared with neutral water or bottom sediments (Anderson 1994; Anderson and Robbins 1998). A relationship between the spectral characteristics of contaminated water and measured pH and Fe_{total} concentrations was found, and proposed to be used for satellite-based or airborne monitoring of mine water pollution of rivers (Alexander et al. 1973; Anderson and Robbins 1998).

The development of hyperspectral imaging (in particular, AVIRIS, HYPERION, and HyMap sensors), substantially expanded the opportunities for remote sensing of water pollution. Swayze et al. (2000) applied the AVIRIS hyperspectrometer to determine secondary minerals containing oxides and hydroxides of iron (indicators of AMD) that are formed as precipitates in acid water. The collection of spectral libraries based on field measurements allowed AMD-affected areas to be identified with image processing algorithms (Riaza et al. 2011). The most detailed analysis of the spectral characteristics of contaminated water has been performed using the HyMap hyperspectrometer. Two spectral reflectance peaks (between 570 and 640 nm, and about 700 nm) of water contaminated by AMD have been found (Riaza et al. 2015). Thus, the red and red edge spectral bands are crucial in detecting AMD-related contamination and in separating polluted water from pure water.

Several studies have focused on the quantitative assessment and mapping of surface water pH in the AMD-affected areas with HyMap hyperspectrometer data (Williams et al. 2002; Zabcic et al. 2009, 2014; Kopačková 2014), based on the detection of secondary minerals that form at different pHs; the results showed the potential of hyperspectral imagery application as an efficient way to monitor AMD.

The Sentinel 2A/2B satellites, launched by the European Space Agency (ESA) in 2015 and 2017, have great potential for monitoring of AMD-related contamination of surface water and its seasonal variation (Kopačková 2019). They provide the data in 8 rather narrow visible and near-infrared (VNIR) spectral bands with a spatial resolution of 10 and 20 m. Another important advantage of the Sentinel-2 mission is its high frequency of obtaining images (in temperate latitudes—every 2–3 days in clear sky conditions). However, only a few studies have focused on the use of Sentinel-2 images for AMD detection and water quality monitoring in coal mining areas (Seifi et al. 2019; Kopačková 2019). So, this study was undertaken to assess the advantages and limitations of the Sentinel-2 satellite data for monitoring AMD-related pollution of surface water in a coal mining area, using the abandoned Kizel coal basin as a case study. Satellite-based assessment of the seasonal variability of water contamination, associated with weather and hydrological environments, was also a focus of this study.

Study Area

The Kizel coal basin stretches for 100 km along the western slope of the Ural Mountains and is characterized by a temperate humid climate. Average annual temperature ranges from 0 to 2°C with a minimum in January (−14 to −16°C) and maximum in July (+16 to +18 °C). Average annual precipitation is 800–900 mm (WorldClim 2.0, Fick and Hijmans 2017). The coal basin area falls within three large basins of the Yayva (with the North Vil'va tributary), the Kos'va, and the Chusovaya (with the Us'va and the South Vil'va tributaries) Rivers (Fig. 1). These three rivers are tributaries of the Kama Reservoir. The annual flow cycle is characterized by a maximum in April or May (related to snowmelt runoff) and two minimums in winter and at the end of summer.

Industrial coal mining in the Kizel coal basin began in the late nineteenth century. By 1959, it had reached a maximum (over 12 million t/year). Subsequently, production began to decline due to the poor quality of coal (in particular, high sulfur levels) and hard mining conditions. Between 1993 and 2000, coal mining was halted and all of the mines in the Kizel coal basin were abandoned. The long-term operation of the mines has led to environmental problems: land disturbance, air pollution, alteration of hydrochemical and hydrological regimes of the rivers, and pollution of surface water and groundwater (Maximovich and Khayrulina 2014; Maximovich and Pyankov 2018; Menshikova et al. 2020).

The mines were completely flooded within 3–10 years after their abandonment, which has led to AMD discharges. There are currently 19 AMD sources in the Kizel coal basin, with an average annual discharge of about 25,000 m^3/h for the period 2007–2013 (Maximovich and Khayrulina 2014; Menshikova et al. 2020). The AMD has total mineralization up to 35,000 mg/L and extremely high concentrations of Fe_{total} (up to 3500 mg/L), Al (up to 190 mg/L) and several trace elements (Maximovich and Pyankov 2018).

The basins of large tributaries of the Kama Reservoir, such as the Yaiva, the Kos'va, and the Chusovaya Rivers, are all affected by the closed mines of the Kizel coal basin. When AMD interacts with surface water, precipitates consisting mainly of iron and aluminum hydroxides form and accumulate on the river bottom (Figs. 2 and 3). It spread for

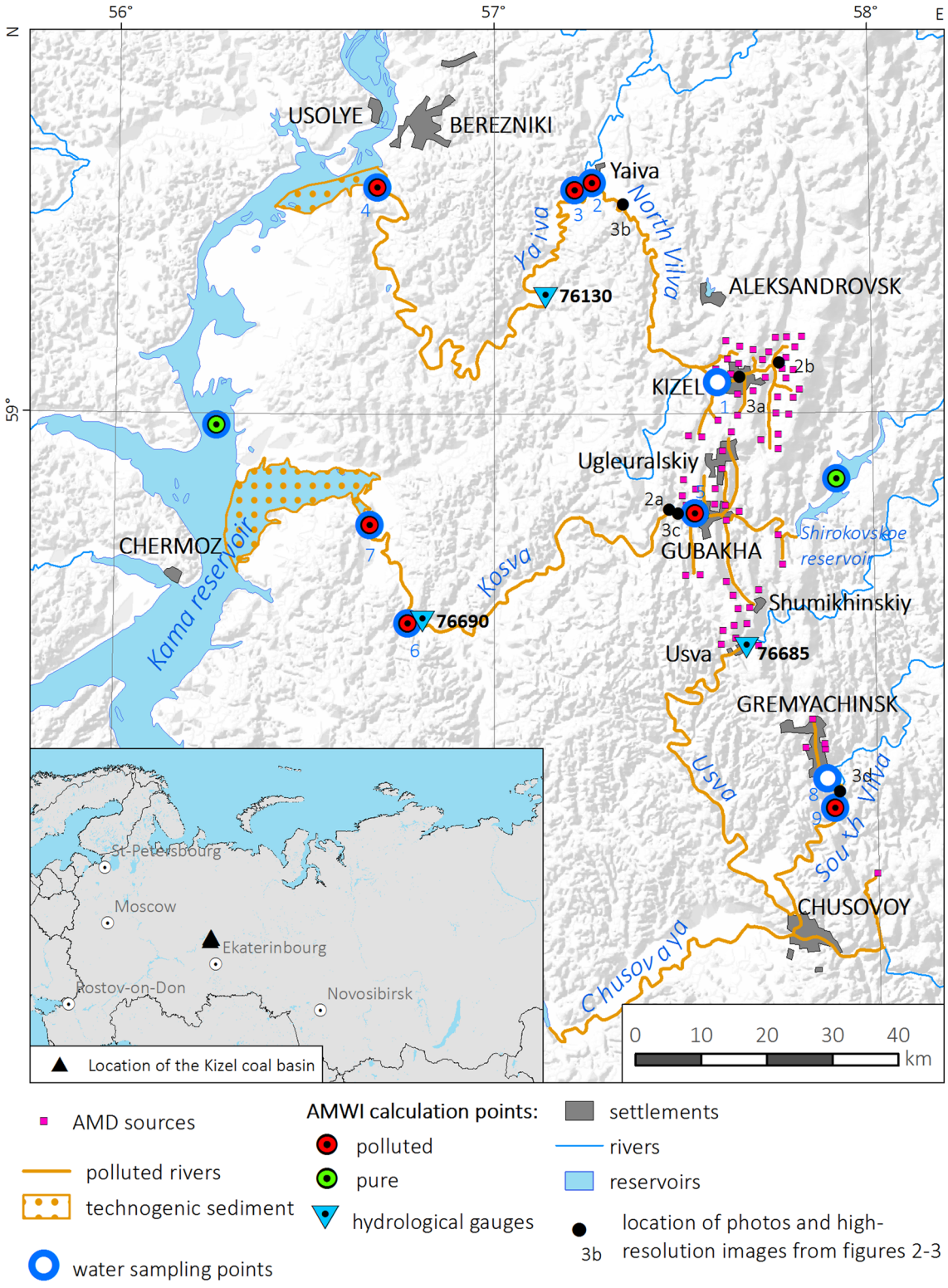

Fig. 1 Location of the Kizel coal basin, contamination sources, and surface water sampling points

hundreds of kilometers downstream up to the Kama Reservoir (Maximovich and Pyankov 2018). The runoff from waste rock dumps is considered to be a second source of river contamination in the Kizel coal basin. Its contribution to the total contamination is estimated at ≈5 % (Maximovich and Pyankov 2018).

Since 2000, the Ural Center of Social and Environmental Monitoring (UCSEM) has been regularly sampling and analysing surface- and ground-water in the Kizel coal basin. Samples are collected and analysed 4–6 times a year during a warm period at 17 AMD sources, as well as at 39 sampling points in polluted rivers (State reports, 2006–2018). The hydrochemical monitoring data for 2006–2018 is published on an online web map service (http://kub.maps.psu.ru/); the main hydrochemical characteristics of the contaminated rivers are shown in Table 1.

The small rivers flowing through the Kizel coal basin (downstream of the AMD sources) are characterized by high concentrations of dissolved and suspended contaminants, exceeding natural values by hundreds of times. Thus, seven AMD sources affect the Bol'shoi Kizel River, a tributary of the North Vil'va River (Fig. 1). The Bol'shoi Kizel River has a "rusty" color (Fig. 3a) due to high concentrations of Fe_{total} (225.5 mg/L). The Bol'shaya Grem'achaya River, flowing through the southern part of the coal basin, is also extremely contaminated (Fe_{total} is 366.3 mg/L) by one powerful AMD source and 20 waste rock dumps. However, unlike the Bol'shoi Kizel River, its contamination has tended to decrease over time (State reports, 2006–2018).

These small rivers are tributaries of larger rivers (the North Vil'va and South Vil'va). The concentration of contaminants in them is substantially reduced due to natural removal processes and dilution, but it remains quite high (up to 42.6 mg/L for Fe_{total}) and optical characteristics of water are greatly altered (Fig. 3b, d). According to the chemical analysis, Fe (III) hydroxide gives the rusty color to the water.

In the Kos'va River basin, there are six AMD sources, and the main ones are located in close proximity to the river. So, downstream of the AMD sources, the water is acid (mean pH is 5.3) and strongly contaminated (Table 1; Fig. 3c). The concentrations of the main pollutants (Fe_{total}, Al, and trace elements) are reduced downstream by several times. However, some reach the Kama Reservoir, and were deposited in the gulf of the Kos'va.

Data and Methods

Overview of the Data Sources

In this study, we used four main data sources to assess the opportunities for satellite-based monitoring of AMD-related contamination of surface water and its seasonal variability in the Kizel coal basin. Their main characteristics are shown in Table 2.

Each data source has some limitations. For the Sentinel-2 images, the main limitation was the low frequency of cloudless images, ranging from two (in 2019) to six images over the warm season. The images taken during periods of heavy rainfall were also excluded from the analysis, since strong water turbidity increases reflectance in the red spectral band, making it hard to distinguish from water contaminated by AMD (Raval 2011).

The hydrochemical monitoring data of UCSEM (Monitoring…, 2006–2018) was obtained for nine sampling points located in six rivers (Table 1; Fig. 1). Due to the low sampling frequency (4–5 times per year), matching of hydrochemical data with Sentinel-2 images is challenging. Furthermore, some of the sampling dates fall on periods of overcast (mainly in autumn). Therefore, only three samples for each year could be matched with the dates when Sentinel-2 images were obtained.

Water samples for determining Fe_{total} were collected in containers made of polymer material and acidified to a pH of less than 2 with hydrochloric acid for preservation. The photometric method with o-fenatropilom was used for laboratory-based analysis of Fe_{total} concentration.

In this study, we used the data provided by the UCSEM, which includes chemical analysis of surface water in the Kizel coal basin. Only the data on Fe_{total} concentration

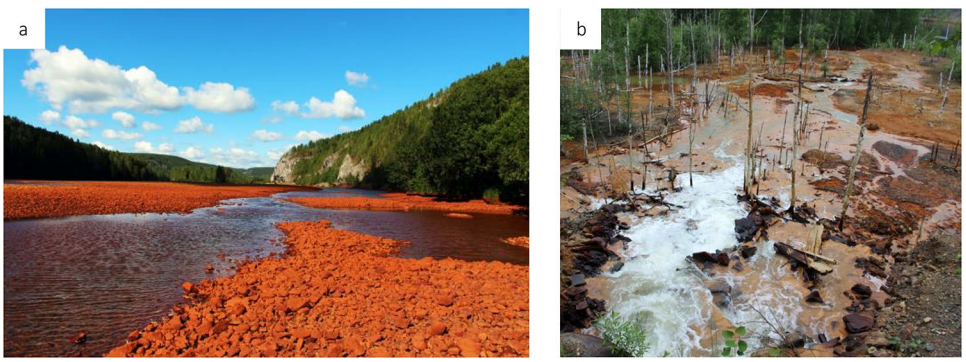

Fig. 2 Contaminated bottom sediments (**a**) and AMD source (**b**)

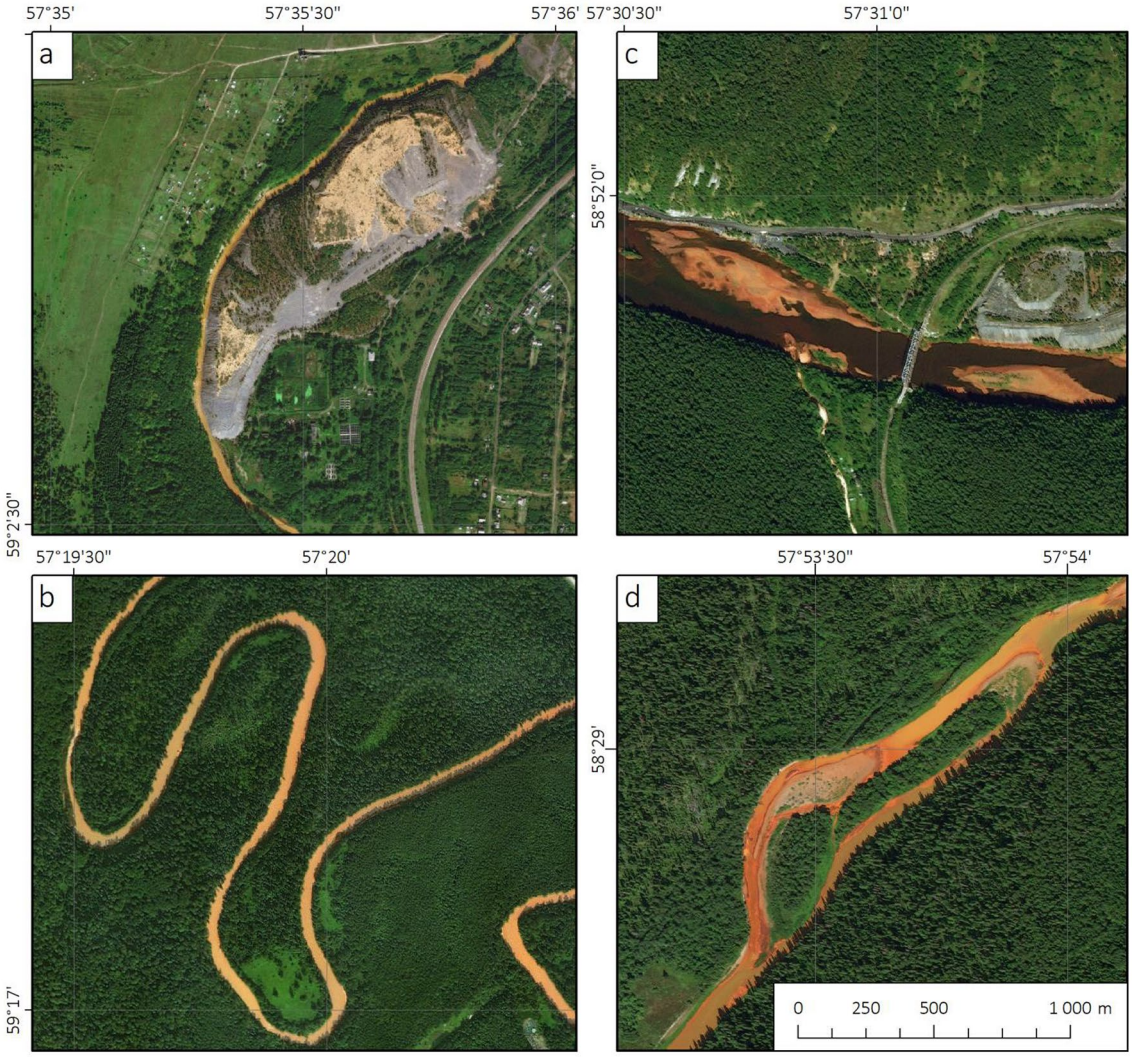

Fig. 3 High-resolution images (obtained from ArcGIS imagery web service) of the rivers and sediments contaminated by acidic mine water in the Kizel coal basin: the Bol'shoi Kizel (**a**), the North Vil'va (**b**), the Kos'va (**c**) and the South Vil'va (**d**)

(without discriminating on Fe^{2+} and Fe^{3+}) were available. Due to the lack of data on Fe^{2+} and Fe^{3+} concentrations and their transformation in contaminated surface water, we performed a measurement of Fe^{2+} and Fe^{3+} in the Kos'va River. It was found that below pH 6.3−7.5, the concentration of Fe^{2+} in the river water was less than 0.05 mg/L (Table 3). The contribution of Fe^{3+} to the total iron concentration in the river water reaches 99 %. So, we assumed that the Fe_{total} concentrations in the surface water, measured by the UCSEM (State reports, 2006–2018), is approximately equal to the Fe^{3+} concentration. The hydrological data were obtained from three gauges (Fig. 1). No such data was available for the North Vil'va and South Vil'va Rivers. Thus, we had to use observations from the nearest hydrological gauges located on the Yayva and Us'va Rivers as analogues.

The precipitation data was obtained from the same hydrological gauges and one weather station. Their main limitation is the low observation density.

Satellite-Based Assessment of AMD-Related Surface Water Contamination

The main feature of the spectra of water contaminated by AMD is a strong increase of reflectance in red and red edge bands (between 650 and 800 nm) compared with blue and green bands (Anderson 1994; Anderson and Robbins 1998). So, several spectral indices based on this difference were developed to distinguish acid water and iron oxide precipitates associated with acid conditions from neutral water and precipitates. The simplest among them is the iron oxide index, which was used to detect ground- and

Table 1 Hydrochemical characteristics of the contaminated rivers of the Kizel coal basin (according to the State reports, 2006–2018)

Sampling point	Point number	Distance from the nearest AMD source, km	Number of samples	pH range and (mean values)	Concentrations, mg/L (range and mean values)					
					Total solids content	SO_4	Al	Fe (total)	Be	Mn
The Bol'shoi Kizel River, downstream of AMD sources	1	11	61	2.6–5.5* (3.15)**	50–3222 (1393)	10–2442 (852)	0.9–34.9 (13.2)	0.86–637.4 (225.5)	0.0002–0.077 (0.0075)	0.15–7.97 (3.48)
The North Vil'va River, near the confluence with the Yayva River	2	84	49	4.2–8 (7.0)	121–630 (430)	20–330 (189)	0.01–2.8 (0.57)	0.05–37.3 (7.9)	0.0001–0.0009 (0.0002)	0.24–1.10 (0.53)
The Yayva river, downstream of the confluence with the North Vil'va River	3	88	52	6.3–8.3 7.4	50–290 (166)	10–120 (42)	0.01–0.7 (0.22)	0.09–5.47 (1.7)	0.0001–0.0002 (0.0001)	0.017–0.24 (0.12)
The Yayva River, near the estuary	4	220	49	6.8–8.3 (7.6)	70–540 (299)	20–175 (54)	0.01–0.09 (0.16)	0.05–5.46 (0.84)	0.0 -0.0003 (0.0001)	0.001–0.15 (0.05)
The Kos'va River, downstream of AMD sources	5	4	46	3.8–6.7 (5.3)	50–292 (144)	10–212 (57)	0.26–1.57 (0.64)	3.87–37.0 (17.3)	0.0001–0.0007 (0.0002)	0.055–0.71 (0.24)
The Kos'va River, near Peremskoe village	6	65	27	6.7–8 (7.5)	64–470 (272)	16–230 (92)	0.04–0.66 (0.25)	0.52–4.58 (2.22)	0.0001–0.0002 (0.0001)	0.03 -0.127 (0.07)
The Kos'va River, near the estuary	7	85	47	6.2–8 (7.4)	57–430 (225)	20–170 (67)	0.02–0.94 (0.24)	0.12–4.17 (1.79)	0.0–0.0003 (0.0001)	0.024–0.16 (0.06)
Bol'shaya Grem'achaya River, downstream of AMD sources	8	1	51	2.7–4.9 (3.2)	132–3790 (1860)	25–2221 (1041)	2.13–63.8 (24.9)	28.1–825.1 (366.3)	0.001–0.0325 (0.014)	0.34–9.57 (3.94)
The Vil'va (south) River, downstream of the contaminated tributary	9	7	52	5.7–7.1 (6.1)	50–415 (128)	10–189 (43)	0.1–1.87 (0.66)	1.72–42.6 (12.0)	0.0001–0.00012 (0.0003)	0.02–0.57 (0.18)

Table 2 The main characteristics of the data sources

Data source	Data provider	Download URL	Period of availability	Temporal resolution	Estimated characteristics
Sentinel-2 images	ESA	https://earthexplorer.usgs.gov/	2016–2019	2–6 cloudless images per year (only for summer-autumn low-water period)	Spectral characteristics of contaminated surface water
Hydrochemical monitoring of surface water	USCEM (State reports, 2006–2018)	http://kub.maps.psu.ru/ (in Russ.)	2016–2018	4–5 samples per year (during the warm period).	pH, total solid content, concentration of Fe, Al and trace elements (Table 1)
Atmospheric precipitation data	Russian hydro-meteorological service (Roshydromet)	https://rp5.ru/ (in (in Russ.)	2016–2019	Every 12 h	Precipitation amount
Hydrological data		https://gmvo.sknii vh.ru (in Russ.)	2016–2019	Every 24 h	Water discharge in rivers

Table 3 Fe^{2+} and Fe^{3+} concentrations in the Kos'va River depending on distance from AMD source and pH values

Name of sampling point	Fe^{2+}, mg/L	Fe^{3+}, mg/L	pH	Distance from the nearest AMD source, km
AMD sources	951.6	3.4	2.5	–
The Kos'va River, downstream of AMD sources	358.9	3.1	6.2	0.005
The Kos'va River	< 0.05	10.7	6.3	4.6
The Kos'va River, near Peremskoe village	< 0.05	0.27	6.5	65.0
The Kos'va River, near Nikylino village	< 0.05	0.133	7.5	84.0

surface- water contaminated by AMD (Yu et al., 2006). After the Sentinel-2 images became available, a new index called $D_{S-2\,(AMD)}$ was suggested to improve identification of precipitates were formed in acidic and neutral conditions (Kopačková 2019). The $D_{S-2\,(AMD)}$ index is calculated as

$$D_{S-2(AMD)} = \left(D_{560} - D_{664}\right) + \left(D_{703} - D_{782}\right)$$

where D_{560}, D_{664}, D_{703}, and D_{782} are the spectral reflectance values in the corresponding bands (3, 4, 5, and 7) of the Sentinel-2 images. This index accounts for the key features of the spectra of acid water and precipitates, but its calculation can be performed only with 20 m spatial resolution (required for resolution of the red edge bands). This spatial resolution may be insufficient to correctly assess the spectral characteristics of rivers having widths less than 20 m. So, the use of 10 m bands (blue, green, red, and near infrared only) may be preferable for some rivers of the Kizel coal basin, namely the North Vil'va and the South Vil'va, which are 15–30 m wide.

In a previous study, we suggested the spectral index called AMWI (Acid Mine Water Index) to assess AMD-related water contamination and its long-term changes in the Kizel coal basin (Berezina et al. 2018). AMWI was calculated as follows:

$$AMWI = \frac{Red - Blue}{Red + Blue},$$

where Red and Blue are spectral reflectance in the red and blue bands respectively. This study was based on the full Landsat archive. We found that the AMWI values increased with increasing iron concentrations in the surface water. The revealed long-term changes in the AMWI were generally consistent with the available data on the intensity of the mine water inflow into the rivers in the 1990s and 2000s (Berezina et al. 2018).

The main limitation of the method was the 30 m spatial resolution of the Landsat images. Therefore, it was implemented only for large rivers with a width of 100 m or more, whereas the most contaminated rivers have a width that are less than 50 m. The frequency of obtaining cloudless Landsat images allowed us to assess only inter-annual variability of the river's contamination, but seasonal variability remained unexplored. In addition, water turbidity, shallow water, ripples, and aquatic vegetation can influence AMWI values and distort their relationship with Fe_{total} concentration in the water. Thus, the use of Sentinel-2 images, which have higher spatial and temporal resolution than Landsat images, may improve the

identification of the river's contamination and especially its seasonal changes.

Satellite Data Processing

In total, 18 images from Sentinel-2 satellites (Level 1 C product) were downloaded for the Yaiva and Kos'va Rivers basins and 16 images for the South Vil'va River basin. All images were obtained between June 5 and September 16. June images were only analyzed in 2019, since an early decline of spring floods that year, and consequently, a decrease in water turbidity was observed.

Preprocessing of the images included transformation from digital numbers to the top-of-atmosphere (TOA) reflectance values and image-based atmospheric correction according to the dark object subtraction method (Chavez 1996). It was carried out with the semi-automated classifier plugin module of the Qgis 3.10 software package.

Then, AMWI was calculated for seven sections of contaminated rivers, located near water sampling points (Fig. 1; Table 1). The sections have areas that range from 1 to 275 ha (depending on the channel's width), and their length ranges from 1.2 to 12 km. They were selected to reduce the influence of external factors that affect AMWI values (especially excluding shallow water areas). In addition, AMWI was calculated for two sections with pure water located in the Kama and Shirokovskoe Reservoirs, which were not affected by the AMD (Fig. 1). The examples of the spectra of surface water with different degrees of contamination are presented in Fig. 4.

To assess the correlation between AMWI values and the hydrochemical/hydrological data, we calculated the Spearman's rank correlation coefficients (ρ), since the obtained observation series were very short (8–9 values of AMWI and Fe_{total} concentration), and their distribution does not correspond to the normal law.

Weather and Hydrological Data

The volume of mine water flowing into the rivers and the amount of surface water contamination substantially varies through a hydrological year (Sarmiento et al. 2009). These variations are determined by hydrometeorological conditions, primarily by the amount of atmospheric precipitation over the previous period and river flow variability. In addition to flow data, we considered the dates of the spring flood peaks (Table 4). Variations in the spring flood peak and dates can also affect mine water drainage and pollutant concentrations (see the "Results" section for more details).

Results

Correlation between AMWI Values and the Fe_{total} Concentration in Surface Water

To assess the applicability of Sentinel-2 satellite data in identifying AMD-related water pollution, we compared the AMWI values with the Fe_{total} concentrations in surface water for the period 2016–2018. Table 5 shows mean, median, and extreme values, and Fig. 5 presents the temporal variability of the AMWI and Fe_{total} concentrations in water.

The highest concentrations of Fe_{total} (mean and maximum) were observed at point 5 (Kos'va River near AMD sources). However, the maximum AMWI values are typically in the South and North Vil'va Rivers (at points 2 and 9), where the concentrations of Fe_{total} in the water was respectively 1.5 and 3 times less than at point 5. For other sampling points, the AMWI values decreased by decreasing the Fe_{total} concentration. Point 4 (the Yayva River near the mouth) is considered to be the least contaminated due to the high flow rates and long distance from the AMD sources (≈220 km).

Temporal variability in Fe_{total} concentration and AMWI values has a high degree of consistency. For 5 out of the 7 sampling points, the Spearman's ρ between AMWI and Fe_{total} concentration in surface water is statistically significant at the 0.05 significance level (ρ = 0.82…0.96), despite the short length of the observation series (8–9 values). No statistically significant correlation between AMWI and Fe_{total} concentration was found at points 4 and 5 (see Table 1).

The inconsistency between high Fe_{total} concentration and relatively low AMWI values at point 5 may be because the Kos'va River near point 5 is very shallow (Figs. 2a and 3c), and bottom sediments can strongly affect AMWI values.

Inter-annual and Seasonal Variability of the AMWI and Water Contamination

The Spearman's ρ between all pairs of observation points for the period 2016–2019 (Table 6) were calculated to assess the synchronicity (coherence) of AMWI variability in the studied rivers. First, there was a statistically significant (at a 0.05 significance level) positive correlation between the AMWI values at the points located within the Yaiva basin (points 2–4) and the Kos'va (points 5–7) Rivers. At these points, changes in the AMWI occurred synchronously due to pollutant input from one cluster of AMD sources. At the same time, the AMWI values at point 5 (the Kos'va River near the town of Gubakha) did not correlate with the observations downstream in the Kos'va River. The correlation between AMWI values and Fe_{total} concentrations at this

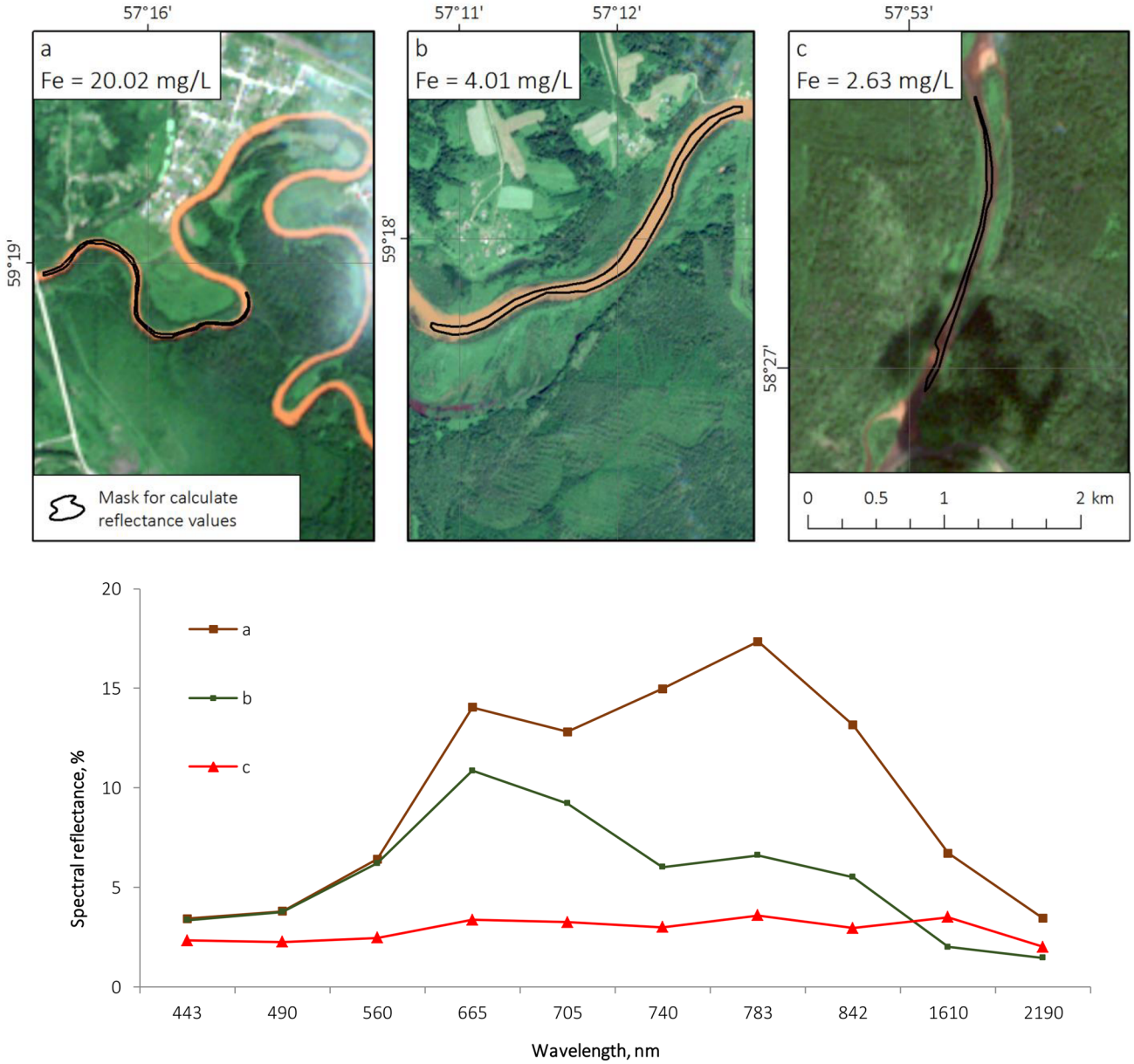

Fig. 4 The sampling areas for AMWI assessment and the spectra of contaminated water (based on the Sentinel-2 image obtained at July 18, 2017): **a** the Vil'va (north) River, near the confluence with the Yaiva River, **b** the Yaiva River, near the confluence with the Vil'va River, **c** the Vil'va (south) River, downstream of the contaminated tributary

Table 4 Several hydrological characteristics of 2016–2019 at the hydrological gauges in the Kizel coal basin

WMO ID of hydrological gauge	Maximum water discharge (m^3/s) and date of the peak of spring flood				Precipitation amount over May – September (mm)			
	2016	2017	2018	2019	2016	2017	2018	2019
76,130	913 (22.04.2016)	1030 (06.05.2017)	959 (23.05.2018)	1248(11.05.2019)	371	500	348	478
76,690	674 (24.04.2016)	782 (06.06.2017)	772 (23.05.2018)	895 (14.05.2019)	211	530	330	540
76,685	349 (19.04.2016)	562 (04.05.2017)	485 (21.05.2018)	521 (10.05.2018)	268	527	474	500

Table 5 The comparison of average, median, and extreme values of the concentration of Fe_{total} with AMWI values (calculated from Sentinel-2 images) for the AMD-affected rivers

No. of sampling point (see Table 1)	Avg., median, and maximum concentration of Fe_{total} (mg/L) for 2016–2018	AMWI values			
		No. of images	mean/median	Max (date of image)	Min (date of image)
2	4.6/3.5/20.0	16	0.37/**0.45**	0.58 (23.07.2018)	− 0.06 (19.08.2016)
3	1.4/1.3/4.0	16	0.18/0.19	0.48 (18.07.2017)	− 0.11 (19.08.2016)
4	0.62/0.44/1.88	14	0.06/0.03	0.32 (05.06.2019)	− 0.15 (19.08.2016)
5	**13.5/14.5/24.0***	15	0.18/0.18	0.33 (19.08.2018)	− 0.02 (19.08.2016)
6	1.3/1.5/2.5	16	0.16/0.17	0.27 (05.06.2019)	0.0 (19.08.2016)
7	1.19/0.83/2.52	15	0.14/0.16	0.28 (05.06.2019)	− 0.04 (19.08.2016)
9	9.4/9.2/16.8	16	**0.39**/0.38	**0.62** (13.07.2016)	**0.14** (15.07.2018)

*The highest values are highlighted

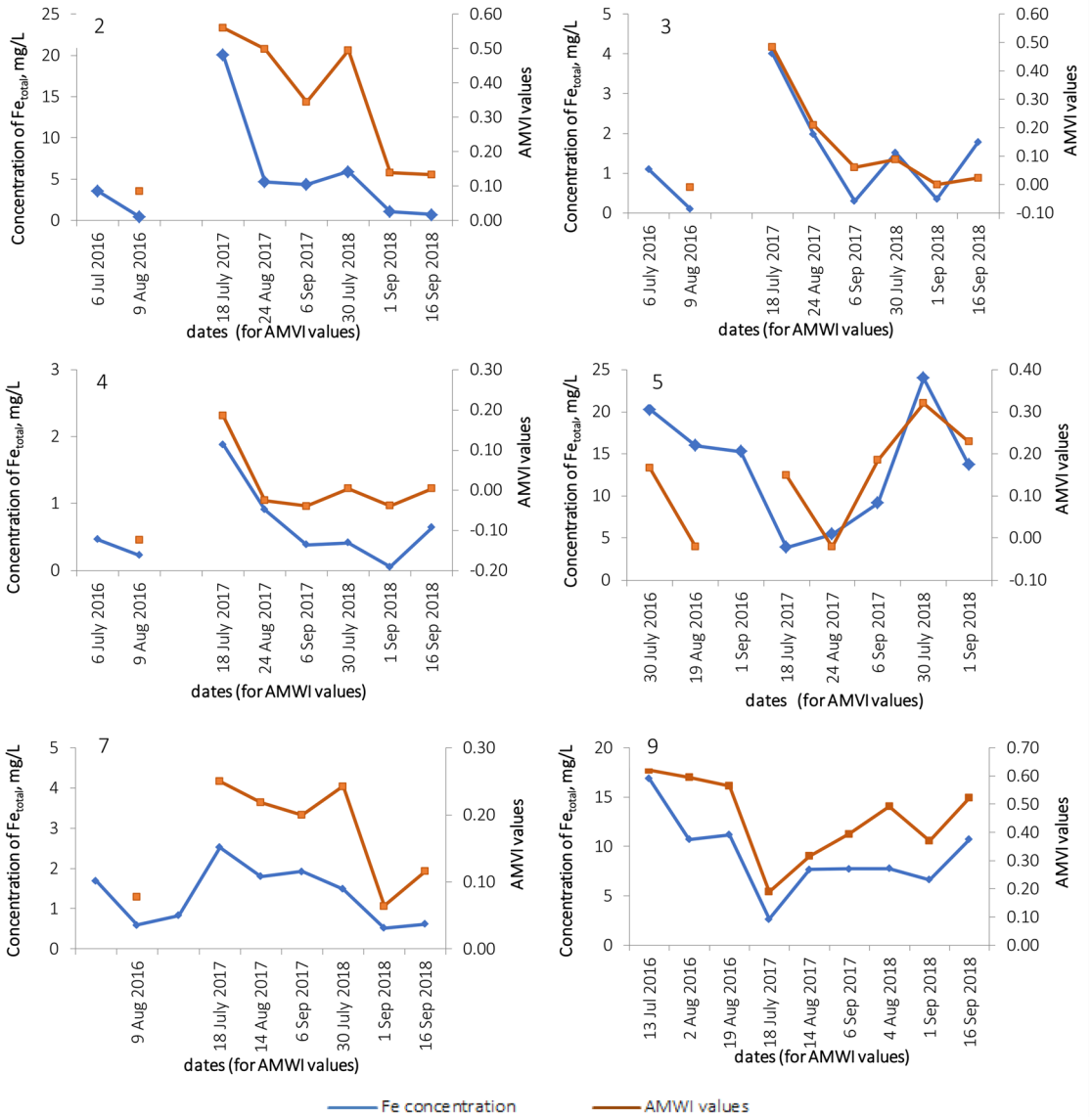

Fig. 5 Variability of the Fe_{total} concentration and AMWI values for the AMD-affected rivers (numbers of points are shown at Fig. 1)

point was also weak (Fig. 5), unlike the downstream observation points.

When comparing the AMWI values between the Yaiva (points 2–4) and the Kos'va (points 5–7) River basins, statistically significant correlations were revealed in most cases, except at point 5. This indicates that the seasonal variability of water contamination in the Yaiva and the Kos'va Rivers was determined by the same patterns.

The AMWI values for the South Vil'va River (point 9) have statistically significant negative correlation with most observation points in the Yaiva and the Kos'va River basins. Thus, the inter-annual and seasonal variability of mine water inflow to the South Vil'va River significantly differs from that of the Yaiva and Kos'va Rivers.

The variability of the AMWI values for the four sampling points on the North Vil'va, the Yaiva, the Kos'va, and the South Vil'va Rivers for 2016–2019 is shown in Fig. 6. The flow at the hydrological gauges is also given to assess its correlation with AMWI variability.

There was a statistically significant positive correlation (at the 0.01 significance level) between the flow rate and AMWI values (the Spearman's ρ was 0.83 and 0.73, respectively) for the Yaiva River (points 3 and 4). For point 6, the correlation of AMWI with the flow rate at the hydrological gauge was also statistically significant ($\rho = 0.69$), unlike at point 5 (Spearman's ρ is −0.15). Statistically significant negative correlation was found between AMWI and the flow rate for the South Vil'va River ($R = -0.83$). However, it is important to note that these correlations were only relevant for the summer low-flow period.

The period under consideration (2016–2019) was characterized by strong fluctuations in the amount of precipitation and rivers runoff for the Kizel coal basin (Table 4). The spring flood in 2016 peaked 15–20 days earlier than the mean dates, according to long-term observations (Georgievsky, 2015). The summer of 2016 was extremely hot and dry; the maximum daily temperature exceeded 30° C during 15–20 days in July and August and the amount of precipitation was only 40–50 % of the mean climatic values. This led to a substantial decrease in flow (by 1.5–2 times comparing with monthly mean flow over August). However, water outflow from the mines was also substantially reduced. As a result, the minimum concentration of Fe_{total} and the lowest AMWI values, according to the Sentinel-2 images, were observed in the Yaiva and Kos'va Rivers in August 2016.

In contrast, the first half of summer 2017 was 2–3° colder than mean climatic values, and the amount of precipitation exceeded climatic values by 1.5–2 times. Water inflow into the mines and, consequently, the AMD discharge was greater than in the same time period in 2016. In mid-July, the Fe_{total} concentration in the rivers reached their maximum. According to the Sentinel-2 image obtained July 18, 2017, the AMWI values were close to their maximum for the entire considered period (2016–2019). In August and September, atmospheric precipitation, river runoff, and then the AMD discharge all decreased, which led to a decrease of AMWI.

In 2018, the spring flood peak was observed in the last third of May, while the summer of 2018 was characterized by close to average temperatures and precipitation. Consequently, no substantial anomalies were observed in river flow. The maximum AMWI for the Yaiva and the Kos'va Rivers were observed in July, i.e. in the first half of the summer low-flow period, because the AMD discharge decreased slower than the river flow. In August and September, the AMD discharge also substantially fell, leading to decreased AMWI values and lower concentrations of Fe_{total} in the surface water.

In 2019, the spring flood peaked near the middle of May. Then, there was a rapid decline in the river's flow, which reduced turbidity. This allowed us to assess AMWI for the North Vil'va, Yaiva, and Kos'va Rivers, and AMWI values were high according to the images obtained on June 5–6, 2019 (Table 5). AMWI then decreased slightly by mid-July. The second half of summer, 2019 within the Kizel coal basin was extremely cloudy and wet; the precipitation amount exceeded climatic values by 2.5 times in August. No cloudless images were obtained after July 20 until mid-autumn.

The fluctuations of the AMWI and Fe_{total} concentrations for the South Vil'va River substantially differ from the same for the Yayva and Kos'va Rivers (Fig. 6c). The highest

Table 6 Spearman's ρ between the values of AMWI in various sampling points (the number of points according to the Table 1)

Point number	2	3	4	5	6	7	9
2	1.00	**0.89**	**0.81**	0.01	**0.65**	**0.84**	**– 0.87**
3	**0.89***	1.00	**0.92**	– 0.14	**0.73**	**0.83**	**– 0.82**
4	**0.81**	**0.92**	1.00	0.24	**0.80**	**0.77**	**– 0.90**
5	0.01	– 0.14	0.24	1.00	0.35	0.35	– 0.12
6	**0.65**	**0.73**	**0.80**	0.35	1.00	**0.80**	**– 0.75**
7	**0.84**	**0.83**	**0.77**	0.35	**0.80**	1.00	– 0.60
9	**– 0.87**	**– 0.82**	**– 0.90**	– 0.12	**– 0.75**	– 0.60	1.00

Statistically significant values (at a 0.05 significance level) are highlighted

*The highest values are highlighted

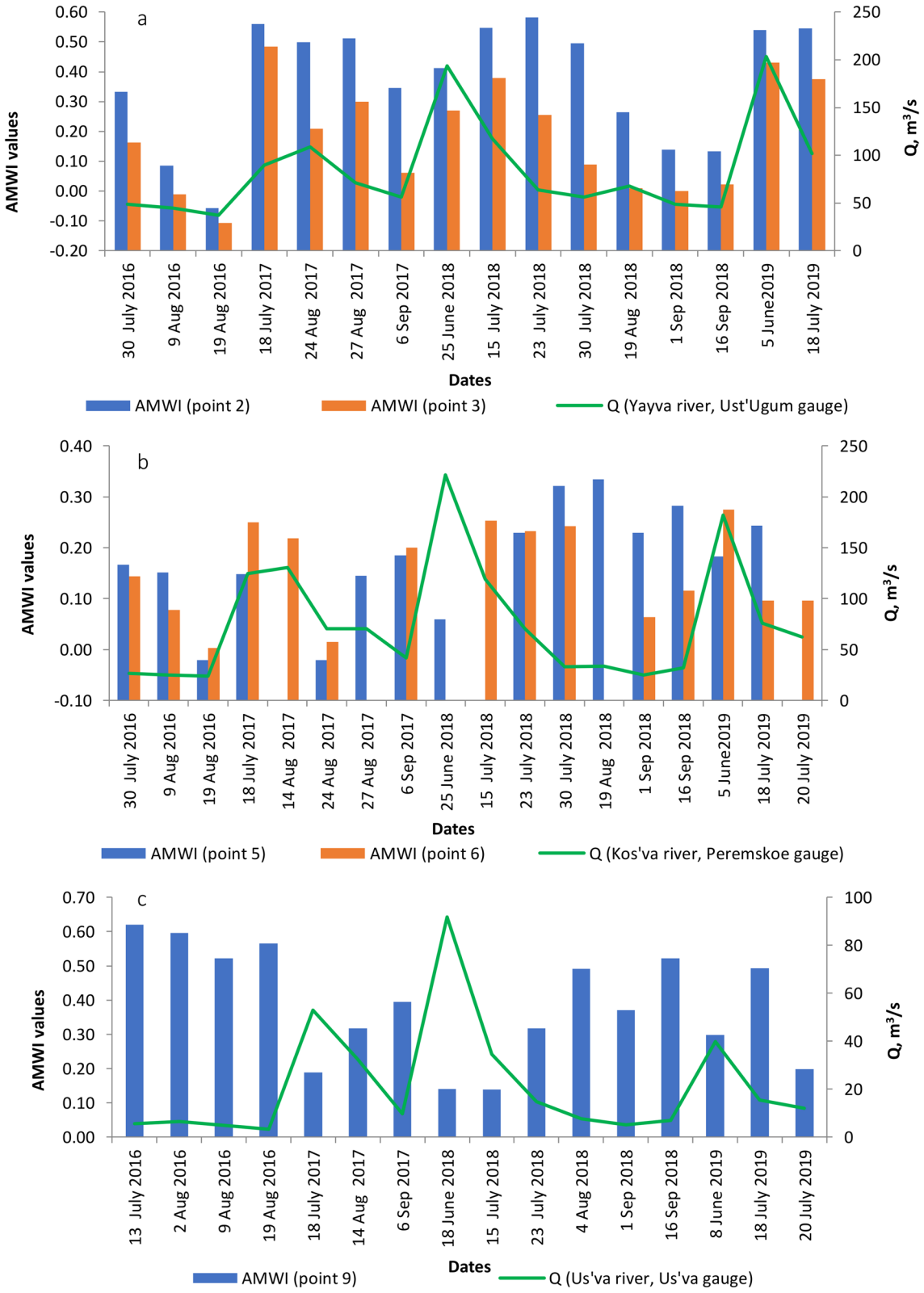

Fig. 6 Variability of the AMWI values (bars) and water discharge (Q, m^3/s) at the river gauges (lines) for the sampling points located in the basins of the Yaiva (**a**), the Kos'va (**b**) and the South Vilva (**c**)

concentration of Fe_{total} was observed during the dry summer of 2016. In subsequent years, flow rates were higher and AMWI values were substantially lower (with some exceptions during the summer of 2018). This variability can be explained by peculiarities of the AMD in the basin of the Vil'va River. During the summer season, the AMD discharge was relatively stable, and the concentration of Fe_{total} in the river increased with decreasing river levels.

Water Contamination Evolution Downstream from AMD Sources, According to the Sentinel-2 Data

A comparison of the AMWI values with Fe_{total} concentration at sampling points located on the Bol'shoi Kizel, North Vil'va, Yaiva, and Kos'va Rivers shows a substantial decrease of contamination with increasing distance from the AMD sources. This phenomenon is due to sedimentation of the pollutants and dilution by pure water coming from tributaries. The bulk of the Fe(III) hydroxide and trace elements were transported and accumulated as sediment in the rivers, creating a zone of highly contaminated bottom sediments that can become sources of secondary pollution as the hydrochemical and hydrodynamic environments change.

Sentinel-2 images provide a continuous assessment of contamination decrease downstream from AMD sources, in contrast to point-based hydrochemical observations. We analyzed changes in surface water contamination along the North Vil'va and the Yaiva Rivers using Sentinel-2 images obtained when the AMWI values were high (July 18, 2017), moderate (July 30, 2018), and low (August 19, 2016). The AMWI was calculated for sections located 10 km from each other, and from the confluence of the contaminated Bol'shoi Kizel River with the Vil'va River to the mouth of the Yaiva River (Fig. 7).

The AMWI values increased along the first 40–60 km downstream from the confluence of the Bol'shoi Kizel River with the Vil'va River. On July 18, 2017, the maximum AMWI values were observed at a greater distance from the AMD source. This might have been due to progressive oxidation of Fe^{2+} cations downstream of the AMD source, as well as the small width and shallow water level of the river (which can allow bottom sediments to substantially affect the AMWI values).

With a low AMD discharge (e.g. August 19, 2016), pollutants mainly oxidize and form sediments before the confluence of the Vil'va and Yaiva Rivers. This is also related to slower flow during low-flow periods. In these environments, only a small portion of the pollutants reached the Yaiva River (Fig. 7b), and the concentration of Fe_{total} in the Yaiva River near the mouth was close to the same as pure water. Buzzi et al. (2016) discovered similar rapid oxidation of precipitated sulphate salts after dry, warm periods and low water levels for the Odiel River in Spain.

With a high AMD discharge (e.g. July 18, 2017), much of the contaminants reached the Yaiva River, where they were gradually diluted and settled. However, the AMWI values exceeded zero when the Yaiva River flows into the Kama Reservoir. According to the hydrochemical data, the concentration of Fe_{total} in the water at the mouth of the Yaiva River (more than 220 km from the AMD sources) reached 1.88 mg/L.

With an average AMD discharge (e.g. July 30, 2018), the AMWI values for the Vil'va River were very high (≥ 0.5); however, they sharply decreased (to zero) downstream of its confluence with the Yaiva River. The AMWI values were below zero at the mouth of the Yaiva River. This indicates that the contaminants generally did not reach the Kama Reservoir.

Discussion

Data and Method Limitations

The use of Sentinel-2 images for AMD mapping and surface water quality assessment in mining areas has both advantages and substantial limitations. The main advantages are public access to the data, its relatively high temporal resolution (3–4 images per week in cloud-free conditions) and the availability of 10 spectral bands in the VNIR region, which provides great potential to identify AMD-related water contamination and precipitates (Seifi et al., 2019). Nevertheless, the use of Sentinel-2 images for monitoring of AMD-related contamination is strongly limited by their coarse spatial resolution (10–20 m). So, only two studies (Kopačková 2019; Seifi et al. 2019) have focused on the use of Sentinel-2 data for AMD mapping, and neither considered water quality. Cloudiness is also a substantial limitation for the use of Sentinel-2 images. For example, only two cloudless images were obtained for each sampling point during the entire summer season of 2019.

Airborne hyperspectral data (Zabcic et al. 2009, 2014; Riaza et al. 2011, 2015; Buzzi et al. 2016) provide higher spatial and spectral resolution, which is crucial for identifying secondary AMD-related minerals, but its use is limited to local areas. In its turn, the use of Sentinel-2 images is most suitable for monitoring AMD for large-scale areas with enough wide (≥ 20 m) contaminated rivers and a low density of ground-based monitoring network. The investigated Kizel coal basin met all of the listed criteria.

The AMWI index, proposed in (Berezina et al. 2018) and used in this study, also has some substantial limitation for water quality assessment, despite the discovered strong correlation with Fe_{total} concentrations in surface water. The

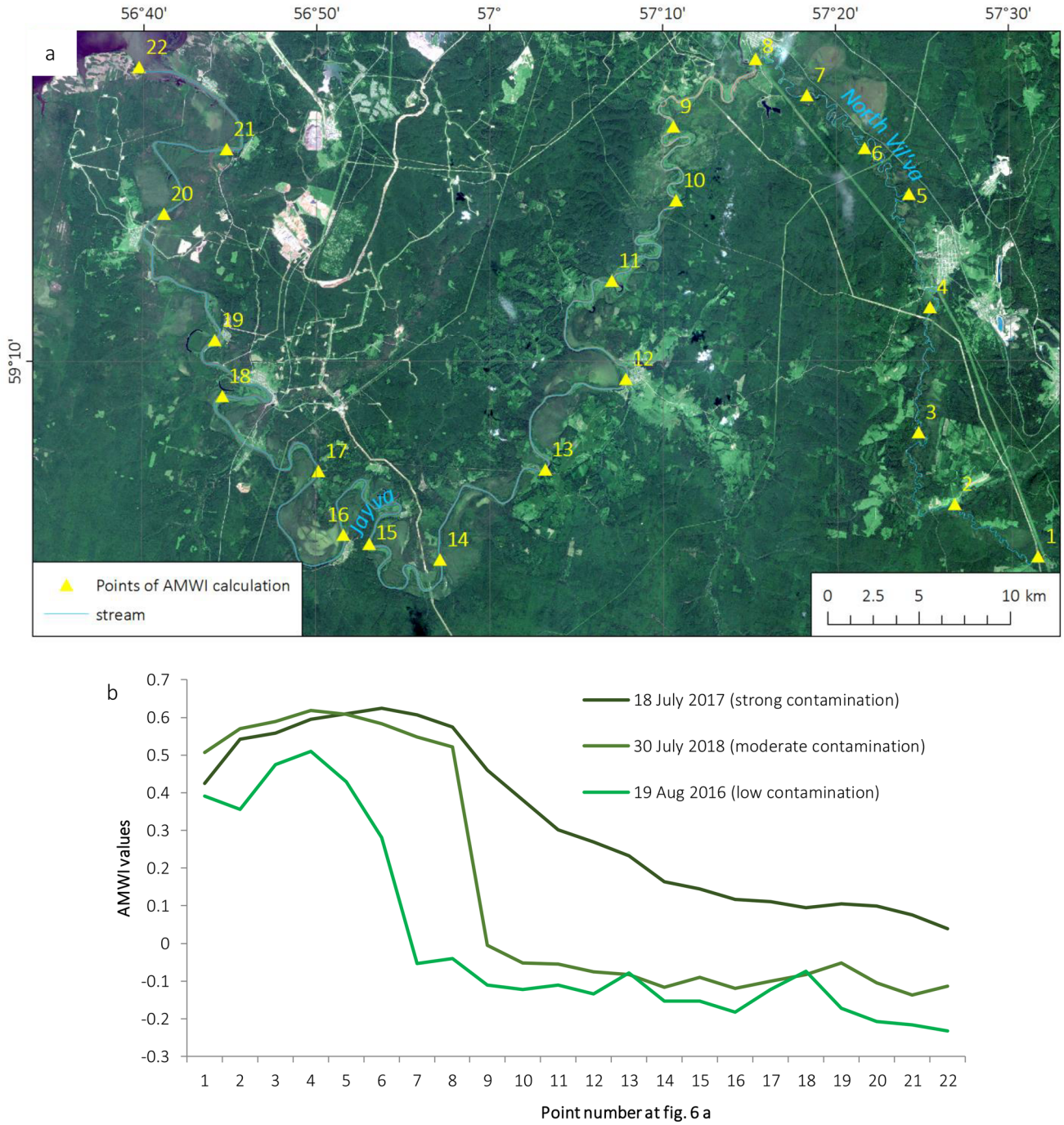

Fig. 7 Decreasing of AMWI values downstream the Vilva and Yaiva Rivers: **a** Sentinel-2 image obtained on July 18, 2017 (natural colors RGB); **b** changes of the AMWI values along the Vilva and Yaiva Rivers, calculated on the images for different dates

nature of the spectral characteristics (the degree to which it reflects the water vs. suspended, bottom, or bank sediments) presents the main uncertainty, greatly affecting interpretation of AMWI values. In accordance with Gammons et al. (2005), one can assume that in quasi-neutral environments, the suspended particles of hydrous ferric oxide (HFO) dominated the total Fe load. Therefore, AMWI values and their seasonal fluctuation may be mainly determined by the concentration of suspended HFO.

The contribution of bottom/bank sediments to the seasonal variability of the AMWI values may be less pronounced than that of suspended HFO. It is important to note that the highest AMWI values were observed 60–70 km downstream of the AMD sources (Fig. 7b), whereas the

areas with dry and strongly contaminated bottom sediments (Fig. 2b) were located closer to them. The open bottom sediments have lower AMWI values than contaminated water with suspended HFO. So, the maximum observed values of AMWI (up to 0.6) may be associated with contaminated water, rather than bottom sediments.

Also, if the spectra was formed mainly by bottom and bank precipitates, then the maximum AMWI values would be observed during low-flow periods, e.g. in August and September, when the largest areas of bottom sediments are uncovered. Actually, the highest AMWI values were observed in July, and then they sharply decreased as water outflow from the mines decreased. Olias et al. (2004) and Sarmiento et al. (2009) also highlighted the substantial contribution of rainfall and flooding to seasonal fluctuations of concentrations of iron and other metals in the surface water.

The inverse correlation between AMWI values and iron concentrations discovered in the South Vil'va River (unlike positive correlations in the North Vilva and Kos'va Rivers) may be because the South Vil'va River is shallower. Consequently, the contribution of contaminated bottom/bank sediments on the spectral characteristics of water surface in South Vil'va River may be higher than for other rivers. Additional field investigations are needed to confirm/reject this hypothesis. Another limitation of the method is the influence of turbidity and wind-induced waves on AMWI values.

Seasonal Changes of AMD Intensity and River Contamination

We have discovered some patterns in inter-annual and seasonal variability of the AMD-related contamination of the rivers in the Kizel coal basin based on combining Sentinel-2 images with hydrochemical monitoring data. The minimum degree of contamination was observed at the end of the dry and hot summer of 2016. This is probably due to the substantial decrease in the discharge of AMD sources, as well as the decrease in the rivers' flow speed. In such environments, the oxidation and sedimentation rate of pollutants increased. In turn, the highest concentrations of Fe_{total} were observed 1–2 months after the spring flood, when the rivers flow decreased more rapidly than the AMD discharge. In general, the volume of mine water flowing into the rivers can be much higher in wet summer seasons. The similar effects of increased AMD discharges induced by heavy rainfall events was previously identified in US (US Environmental Protection Agency 1994) and Spain (Olias et al. 2004; Sarmiento et al. 2009) based on hydrochemical sampling data. Buzzi et al. (2016) also applied remote sensing data (HyMap images) to assess seasonal variability of AMD. They found that the changes in the water level of a river (due to precipitation) explain the geochemical evolution of the precipitates from AMD from dissolved pyrite weathering products. Similar effects were found for the rivers in the Kizel coal basin.

Conclusions

Despite the above-mentioned limitations and uncertainties, our results confirm the efficiency of using Sentinel-2 images to monitor AMD-induced river contamination in coal mining areas. Spatial and temporal resolution of satellite data allowed us to assess the inter-annual and seasonal variability of contamination, even though the hydrochemical monitoring data was fairly sparse and unrepresentative. Statistically significant correlation between Fe_{total} concentration and the spectral characteristics of the water surface estimated by Sentinel-2 images was confirmed for most of the sampling points. The correlation was significant except when the sampling point was far from the AMD sources (over 200 km) or in close proximity to them. Thus, Sentinel-2 images can be considered as the important data source to improve water quality monitoring system in the Kizel coal basin.

In comparison with other remote-sensing based studies of AMD, our approach is only applicable for relatively large contaminated rivers with widths exceeding 20 m. Additionally, the discovered correlation between Fe_{total} concentration and AMWI values is only relevant for quasi-neutral water in which the Fe^{3+} strongly predominates over Fe^{2+}. Yet, if these limitations are satisfied, our method can be used to monitor AMD in other coal basins and sulfide deposits. Currently, this method is being used to study seasonal pollutant migration and accumulation for the Kos'va River.

Acknowledgements This study was funded by the Ministry of High Education and Science of the Russian Federation project 2019 – 0858 and RFBR Projects 17-05-41114 and 19-05-50073.

References

Alexander SS, Dein J, Gold DR (1973) The use of ERTs-1 MSS data for mapping strip mines and acid mine drainage in Pennsylvania. Proc, Symp on Significant Results Obtained from the Earth Resources Technology Satellite 1). NASA, Washington, pp 569–575

Anderson JE (1994) Spectral characterization of acid-mine and neutral drainage bacterial precipitates and their relationship to water quality in a piedmont watershed. Va J Sci 45(3):175–186

Anderson JE, Robbins EI (1998) Spectral reflectance and detection of iron-oxide precipitates associated with acidic mine drainage. Photogramm Eng Rem Sens 64:1201–1208

Berezina OA, Shikhov AN, Abdullin RK (2018) The use of multitemporal satellite images for environmental assessment in coal mining areas (by example of closed Kizel coal basin). Curr Prob Remote Sens Earth Space 15(2):144–158 [in Russian]

Burrell R, Whitworth K (2000) The influence of mine water recovery on surface on gas and water discharges in the Yorkshire Coalfield.

In: Proceedings of the 7th International Mine Water Assoc Congress, pp 81–90
Buzzi J, Riaza A, García-Meléndez E, Carrère V, Holzwarth S (2016) Monitoring of river contamination derived from acid mine drainage using airborne imaging spectroscopy (HyMap data, southwest Spain). River Res Appl 32(1):125–136
Chavez PS Jr. (1996) Image-based atmospheric corrections—revisited and improved. Photogramm Eng Rem Sens 62(9):1025–1036
Demchak J, Skosen J, McDonald L (2004) Distribution and behavior of heavy metals in a river polluted by acid mine drainage in the Dabaoshan mine area, China. J Environ Qual 33(2):656–668
Donovan JJ, Leavitt BR, Werner E (2003) Long-term changes in water chemistry as a result of mine flooding in closed mines of the Pittsburgh coal basin, USA. Proc, 6th ICARD, pp 869–875
Fick SE, Hijmans RJ (2017) WorldClim 2: new 1-km spatial resolution climate surfaces for global land areas. Int J Climatol 37:4302–4315
Gammons CH, Nimick DA, Parker SR, Cleasby TE, McCleskey RB (2005) Diel behavior of iron and other heavy metals in a mountain stream with acidic to neutral pH: Fisher Creek, Montana, USA. Geochim et Cosmochim Acta 69(10):2505–2516
Georgievsky V, Yu (2015) The main hydrological characteristics river basins of the Kama River Reference Book. Moscow, p 135 **[in Russian]**
Johnson DB, Hallberg KB (2005) Acid mine drainage remediation options: a review. Sci Total Environ 338:3–14
Kopačková V (2014) Using multiple spectral feature analysis for quantitative pH mapping in a mining environment. Int J Appl Earth Obs Geoinf 28:28–42
Kopačková V (2019) Mapping acid mine drainage (AMD) and acid sulfate soils using Sentinel-2 data. In: Proceedings of the IGARSS 2019–2019 IEEE International. Geoscience and Remote Sensing Symp, pp 5682–5685
Maximovich NG (2018) Pyankov SV (2018) The Kizel Coal Basin: Environmental Problems and Solutions. Perm State University, Perm (**In Russian**)
Maximovich NG, Khayrulina EA (2014) Artificial geochemical barriers for environmental improvement in a coal basin region. Environ Earth Sci 72:1915–1924
Menshikova E, Osovetsky B, Blinov S, Belkin P (2020) Mineral formation under the influence of mine waters (the Kizel Coal Basin, Russia). Minerals 10:364. https://doi.org/10.3390/min10040364
Monitoring of the socio-environmental impacts of the mines closure in the Ural region (2006–2018). State reports **[in Russian]**
Okamoto M, Kobayashi T, Sakamoto M (2006) Physical properties of sediments deposited in the minewater from a closed coal mine. In: Proceedings of the 10th Congress of the International Assoc for Engineering Geology and the Environment (Electronic resource), Nottingham, UK. Electronic optical disks (CD-ROM)
Olías M, Nieto JM, Sarmiento AM, Cerón JC, Cánovas CR (2004) Seasonal water quality variations in a river affected by acid mine drainage: the Odiel River (south west Spain). Sci Total Environ 333(1–3):267–281
Powell JD (1988) Origin and influence of coal mine drainage on streams of the United States. Environ Geol Water Sci 11:141–152
Raval S (2011) Investigation of mine environmental monitoring with satellite based sensors. PhD Thesis. School of Mining Engineering, The University of New South Wales, Sydney
Riaza A, Buzzi J, García-Meléndez E, Carrère V, Müller A (2011) Monitoring the extent of contamination from acid mine drainage in the Iberian pyrite belt (SW Spain) using hyperspectral imagery. Remote Sens 3(10):2166–2186
Riaza A, Buzzi J, García-Meléndez E, Carrère V, Sarmiento A, Müller A (2015) Monitoring acidic water in a polluted river with hyperspectral remote sensing (HyMap). Hydrol Sci J 60(6):1064–1077
Sarmiento AM, Nieto JM, Olías M, Cánovas CR (2009) Hydrochemical characteristics and seasonal influence on the pollution by acid mine drainage in the Odiel river Basin (SW Spain). Appl Geochem 24(4):697–714
Seifi A, Hosseinjanizadeh M, Ranjbar H, Honarmand M (2019) Identification of acid mine drainage potential using sentinel 2a imagery and field data. Mine Water Environ 38:707–717
Siddharth S, Jamal A, Dhar BB, Shukla R (2002) Acid-base accounting: a geochemical tool for management of acid drainage in coal mines. Mine Water Environ 21:106–110
Swayze GA, Smith KS, Clark RN, Sutley SJ, Pearson RM, Vance JS, Hageman PL, Briggs PH, Meier AL, Singleton MJ, Roth S (2000) Using imaging spectroscopy to map acidic mine waste. Environ Sci Technol 34(1):47–54
Tao X, Wu P, Tang C, Liu H, Sun J (2012) Effect of acid mine drainage on a karst basin: a case study on the high-As coal mining area in Guizhou province, China. Environ Earth Sci 65(3):631–638
Valente TM, Gomes CL (2009) Occurrence, properties and pollution potential of environmental minerals in acid mine drainage. Sci Total Environ 407(3):1135–1152
Williams DJ, Bigham JM, Cravotta CA III, Traina SJ, Anderson JE, Lyon JG (2002) Assessing mine drainage pH from the color and spectral reflectance of chemical precipitates. Appl Geochem 17:1273–1286
Wobber FJ, Russell OR, Deely DJ (1975) Multiscale aerial and orbital techniques for management of coal-mined lands. Photogrammetria 31(4):117–133
Wolkersdorfer C, Nordstrom DK, Beckie RD, Cicerone DS, Elliot T, Edraki M, Valente T, França SCA, Kumar P, Lucero RAO, Soler AIG (2020) Guidance for the integrated use of hydrological, geochemical, and isotopic tools in mining operations. Mine Water Environ 39(2):204–228
Yu S, Chen Z, Wang Y (2006) Application of multi-sensor image in monitoring mining activities and related environment changes: a case study at Daye, Hubei, China. In: Proceedings of the SPIE – The Int Soc for Optical Eng 6200, Art. No. https://doi.org/10.1117/12.682167
Zabcic N, Rivard B, Ong C, Muller A (2009) Using airborne hyperspectral data to characterize the surface pH of pyrite mine tailings. In: Proceedings of the First Workshop on Hyperspectral Image and Signal Processing: Evolution in Remote Sensing, pp 154–157
US EPA (U.S. Environmental Protection Agency) (1994) Acid Mine Drainage Prediction. EPA 530-R-94-036, https://www.epa.gov/sites/production/files/2015-09/documents/amd.pdf. Accessed 16 Sept 2020